UNIVERSITÀ DEGLI STUDI FIRENZE

FLORE
Repository istituzionale dell'Università degli Studi di Firenze

Identification of the main hydrodynamic parameters of Typhoon AUV from a reduced experimental dataset

Questa è la Versione finale referata (Post print/Accepted manuscript) della seguente pubblicazione:

Original Citation:
Identification of the main hydrodynamic parameters of Typhoon AUV from a reduced experimental dataset / Allotta, Benedetto; Costanzi, Riccardo; Pugi, Luca; Ridolfi, Alessandro. - In: OCEAN ENGINEERING. - ISSN 0029-8018. - ELETTRONICO. - 147:(2018), pp. 77-88. [10.1016/j.oceaneng.2017.10.032]

Availability:
This version is available at: 2158/1101366 since: 2021-03-30T15:11:07Z

Published version:
DOI: 10.1016/j.oceaneng.2017.10.032

Terms of use:
Open Access
La pubblicazione è resa disponibile sotto le norme e i termini della licenza di deposito, secondo quanto stabilito dalla Policy per l'accesso aperto dell'Università degli Studi di Firenze (https://www.sba.unifi.it/upload/policy-oa-2016-1.pdf)

Publisher copyright claim:
Conformità alle politiche dell'editore / Compliance to publisher's policies

Questa versione della pubblicazione è conforme a quanto richiesto dalle politiche dell'editore in materia di copyright.
This version of the publication conforms to the publisher's copyright policies.

(Article begins on next page)

12 October 2024

*REVISED Manuscript UNMARKED
Click here to view linked References

DOI: 10.1016/j.oceaneng.2017.10.032

Identification of the main Hydrodynamic Parameters of Typhoon AUV from a reduced experimental dataset

Benedetto Allotta*, Riccardo Costanzi**, Luca Pugi*, Alessandro Ridolfi*

*Department of Industrial Engineering
University of Florence
Florence, Italy
benedetto.allotta@unifi.it, luca.pugi@unifi.it,
a.ridolfi@unifi.it

**DII - Dipartimento di Ingegneria dell'Informazione and
Centro di Ricerca "E. Piaggio"
Università di Pisa
Pisa, Italy
riccardo.costanzi@unipi.it

***Abstract* – In this research work a case study dealing with the identification of the main hydrodynamic properties of an Autonomous Underwater Vehicle (AUV) is presented. The vehicle is the Typhoon-class AUV developed by the Department of Industrial Engineering of the University of Florence, Italy. The identification of the main hull hydrodynamic parameters is very important for the tuning of an accurate dynamic model of the vehicle, which could be used for several purposes including the development of model based localization and navigation filters. The authors describe the simplified identification procedure adopted for the Typhoon AUV starting from a reduced experimental dataset obtained during some missions at sea performed in 2014 in Biograd na Moru, Croatia.**

I. INTRODUCTION

An accurate modelling of the dynamic response of the propellers/thrusters used to control ROV (Remotely Operated Vehicles) and **AUV (Autonomous Underwater Vehicles)** is fundamental to obtain a meaningful simulation of the behavior of the vehicle and in particular for the realistic simulation of the vehicle navigation and control systems. Possible applications range from model based navigation and localization systems to estimation filters for the prediction of partially unknown disturbances such as marine currents. **An almost complete review** about these topics is presented by the work of Saeedi [1].

Typically, two complementary aspects of the problem are investigated:

- identification of the hydrodynamic coefficients of the hull;
- identification of the behavior of the thrusters and of the whole propulsion system.

For the description of the hydrodynamic behavior of the hull a classical approach is summarized by the work of Fossen [2]. Hydrodynamic coefficients describing the behavior of the vehicle can be first approximated using simplified correlations available on handbooks [3][4]. More recently, thanks to the development of CFD (Computational Fluid Dynamics) tools many works have been focused on FEM (Finite Element Method) models for the calculation of hydrodynamic coefficients of vehicles hulls [5] .

However, even considering the recent improvement of CFD sciences, there is still the need of an accurate identification of the vehicle behavior starting from experimental results: in recent works the identification of the vehicle parameters is performed with different techniques such as Kalman filtering [6], neural networks [7], or modal techniques based on the concept of self-oscillations [8].

The reason for such an interest in experimental identification techniques, despite the recent progress of CFD calculations, can be easily understood considering the following factors:

- real Hydrodynamic behavior of an AUV can be heavily affected by various unmodelled phenomena, including the interaction with the propulsion system which still represents a quite hard task for numerical models;
- most of the AUV currently adopted for scientific research have a modular architecture involving variable geometric and mass properties according to the mission profile.

The identification of the behavior of the propellers and thrusters is very important since the behavior of the propellers, in terms of developed thrusts and corresponding reaction torques transmitted to the hull, is influenced by the surrounding field of motion of the fluid and thus by the interaction with the hull dynamics. In particular, in literature the problem is studied in the following terms:

- steady state response of the propellers is studied taking into account different operational conditions and considering single quadrant operation (positive propulsion effort related to a positive direction of motion), or four quadrant operations (arbitrary sign of the propulsion effort with respect to an arbitrary direction of motion) [9]. Typically both kind of responses could be calculated from

CFD models [10]-[12] or from experimental identifications campaigns such as in the work of Pivano [13] or basing on historical data, e.g. the Wageningen profiles originally produced by Oerstveld [14][15] and continuously updated for more recent profiles [16]. In particular, the first quadrant behavior is often approximated using the bilinear law [17] also adopted by Fossen [2], often referred to a simplified dynamic model [18];

- transient response: steady state response of the propeller can be further refined considering time transient introduced by inertial behavior of the propeller driveshaft coupled with the dynamic behavior of the motor [2][17];
- sensitivity to cross fluxes: high cross fluxes of water (associated to relevant kinetic energy) are able to influence the behavior of the propeller. This cross coupling effect is well known and widely discussed in literature: most of the sources [19]-[25] agree that a general approach is difficult to be proposed and simplified models have to be carefully calibrated basing on the experimental evidence of the specific application at hand.

Compared to previous studies and over-cited literature, the authors focused their attention on the identification of the main hydrodynamic parameters of Typhoon AUV (Autonomous Underwater Vehicle) including the analysis of its propulsion system. This vehicle has been developed and built by the Mechatronics and Dynamic Modelling Laboratory (MDM Lab), Department of Industrial Engineering (DIEF), University of Florence (UNIFI), Italy.

Typhoon AUV, visible in Figure 1, is an innovative torpedo-shaped AUV dedicated to localization, investigation and surveillance of archeological underwater sites whose design and simulation have been already discussed in previously published works [26].

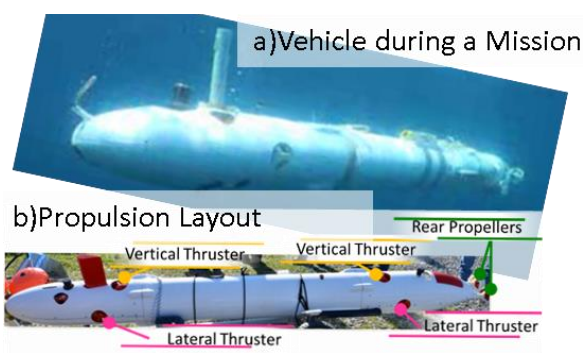

Figure 1: Typhoon AUV: the vehicle during a mission a), and its propulsion system layout b)

The propulsion system layout is visible in Figure 1: two rear propellers are used for standard-straight navigation (they also contribute to the control of the yaw angle) and four tunnel thrusters (two vertical and two lateral) are used to control vehicle orientation or to perform hovering over an assigned target. Considering the high number of controlled independent actuators, six in the example of Typhoon, fixed pitch propellers are adopted in order to reasonably reduce costs and increase the reliability of the whole system. This propulsion system layout, or similar ones, is adopted also by many existing AUVs such as C-Scout [27], Remus [28], Proteus [29], Delphin2 [30] and finally MARTA [31][32], a modular development of the original Typhoon design concept, which has been developed by the University of Florence as a part or the European project ARROWS [37]. It is also interesting to notice the possibility of further extension of this work to the study of the propulsion layout of ROV; typical layouts are given in Figure 2.

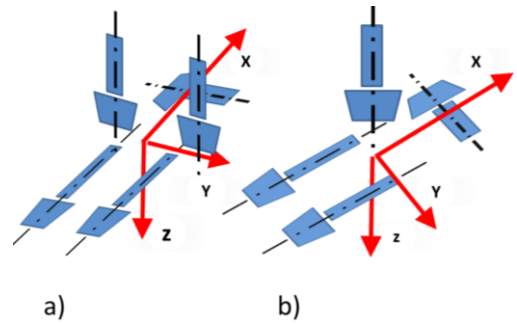

Figure 2: examples of propulsion layouts commonly used for ROVs

To summarize, the main aim of this work is to propose identification procedures that should be considered as a reasonable trade-off between simplified and generalized simulation models and the huge amount of numeric simulations and experimental activities available in literature. In particular, the authors tried to optimize the proposed procedure in order to minimize time and costs needed to reasonably identify and reproduce the dynamic behavior of a real AUV. *Besides this, the identified model, even if simplified with respect to the complete set of dynamics characterizing the considered vehicles, can play a fundamental role for several different applications. E.g. the longitudinal dynamic model is the basis for a prediction on the energy consumption associated to survey missions of AUVs. On the basis of the knowledge of the surge dynamic behavior of the vehicle, from the kinematic constraints, it is possible to predict the coverage associated to a full charge of the batteries. In a similar way, it is possible to design the not constrained kinematic quantities (e.g. the cruise speed) associated to a mission e.g. to maximize the covered area [26]. Another example of application where a dynamic model, even if simplified, could play a valuable role is in the navigation filter of underwater robots. These modules of the motion control system, usually based on Kalman theory, commonly use kinematic models for the prediction of the vehicle behavior and the signal of available sensors for the correction of the estimated state. The introduction of the knowledge of a dynamic model, even if identified exploiting elementary trajectories, is an added value also for the estimation of the navigation state when the vehicle travels along more complex paths.*

II. Modelling of the Hydrodynamic behavior of the Hull

The hydrodynamic behavior of the hull is analyzed following the classical approach proposed by Fossen [2]. SNAME notation corresponding to body and fixed reference systems is described in Figure 3 .

Hull dynamics is accordingly described with respect to a body constrained reference system by (1):

$$M\dot{\nu}+C(\nu)\nu+D(\nu)\nu+g(\eta)=\tau \qquad (1)$$

Where the following symbols are adopted:

- M matrix (6x6) accounting for pure inertial effects;
- C matrix (6x6) corresponding to the contribution of centrifugal and Coriolis effects;
- D matrix (6x6) for the viscous/dissipative effects;
- g vector (6x1) corresponding to the volumetric forces: the gravitational one (the weight) and the buoyancy;
- τ vector (6x1) for the external forces and torques (2):

$$\tau=\left[\tau_1^T,\tau_2^T\right]^T; \quad \tau_1=[X,Y,Z]^T; \quad \tau_2=[K,L,M]^T \qquad (2)$$

- pose and speed vectors η,ν are defined respectively according to (3) and (4): the corresponding reference systems are described in Figure 3.

$$\eta=\left[\eta_1^T,\eta_2^T\right]^T; \quad \eta_1=[x,y,z]^T; \quad \eta_2=[\phi,\theta,\psi]^T \qquad (3)$$

$$\nu=\left[\nu_1^T,\nu_2^T\right]^T; \quad \nu_1=[u,v,w]^T; \quad \nu_2=[p,q,r]^T \qquad (4)$$

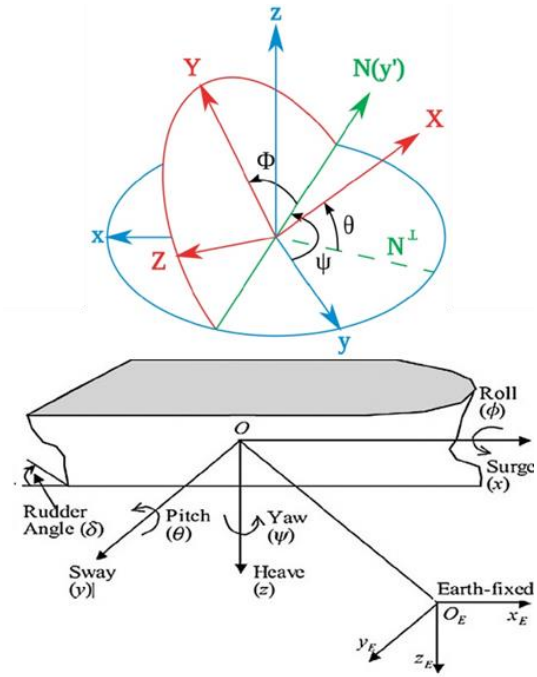

Figure 3: adopted reference systems and notation

The main aim is to exploit a limited set of data, experimentally collected from different simple trajectories, i.e. elementary motions along the main degrees of freedom without exciting cross dynamics. This approach permits the Identification of the main Hydrodynamic Parameters (i.e. some of the diagonal terms in the matrices defined in the standard equations of motions for an underwater vehicle as described in [2]). According to the target methodology, the chosen trajectories are linear paths (surge and heave) and rotations on the spot (yaw).

As clearly visible in the scheme of Figure 4, a typical point to point navigation can be decomposed in a sequence of elementary motions that can be summarized in the following three categories:

- elementary heave motion: starting from an assigned depth the vehicle perform a vertical trajectory (e.g. from the surface, the vehicle reaches an assigned operational depth to start the mission). Considering this particular motion the dynamic behavior of the system corresponding to the system of equations (1) can be simplified to (5):

$$M_{33}\dot{w}+D_{33}(w)w+g_3=Z \qquad (5)$$

  where M_{33} and D_{33} are respectively the elements corresponding to the third row and the third column of the matrix M and D, g_3 represents the third element of the g vector.
  Since most of torpedo-shaped vehicles like Typhoon are approximately axial-symmetric the identified M_{33} and D_{33} coefficient should be almost similar if not identical to M_{22} and D_{22} ones.
- elementary surge motion: vehicle advances along x direction (no or negligible rotation allowed) which

typically corresponds to the more efficient direction of motion. The corresponding simplified equation representing its dynamic behavior is (6):

$$M_{11}\dot{u} + D_{11}(u)u = X \tag{6}$$

In (6) the contribution of g vector corresponding to longitudinal forces is neglected since this contributions is typically null or negligible.

- elementary yaw rotation: the vehicle performs a pure rotation around its vertical axis, holding its current position. The dynamic behavior of the vehicle is approximated by a single scalar equation (7):

$$M_{66}\dot{r} + D_{66}(r)r = M \tag{7}$$

Also in this case the contribution of volumetric forces g_6 is null or negligible.

In Figure 5 a typical example of simple mission profile performed by Typhoon AUV during some tests performed in October 2014 in Biograd na Moru, Croatia (in the framework of the European ARROWS project) is shown: the vehicle performed a square closed loop trajectory which can be easily decomposed in a sequence of the above described elementary motions. In particular, the vehicle starts moving on surface from WP1 (green line in Figure 5); then at WP3 through an elementary heave manoeuvre the vehicle reaches the operating depth and starts its underwater mission in order to reach in sequence WP4 and WP5 where the vehicle returns to surface (red line in Figure 5).

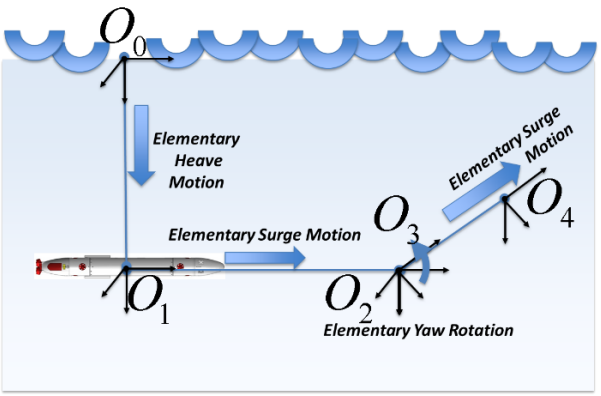

Figure 4: point to point motion and decomposition in a sequence of elementary motions

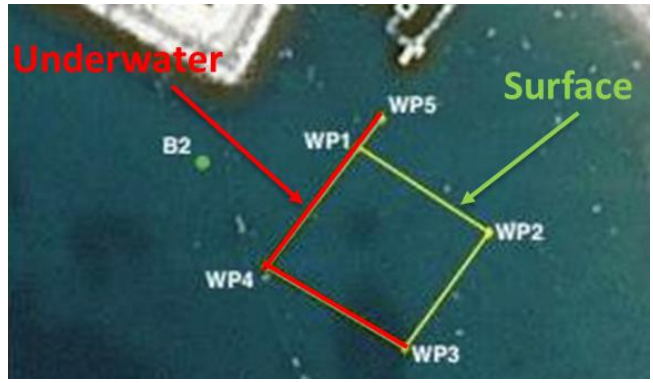

Figure 5: the mission path during experimental tests performed in Croatia, October 2014

The vehicle during the test *was* equipped with a DVL (Doppler Velocity Log) measuring the absolute AUV speed with respect to the sea bottom, as visible from the experimental data reported in Figure 6 (longitudinal speed). The vehicle is also equipped with a commercial IMU (Inertial Measurement Unit) and with a single-axis FOG (fibre optic gyro) to estimate the 3D vehicle accelerations and rotations thanks to a suitable algorithm [38]. It is worth noting in the results of Figure 6 that the measurement of the longitudinal speed during an in place rotation is not completely null: the explanation of such phenomenon could be easily understood considering the following aspects:

- presence of limited underwater disturbances (currents);
- residual errors of vehicle navigation loop;
- mounting position of the sensors and residual bias errors.

In particular the behavior of the vehicle control loop is clearly the cause of the recorded vehicle speed overshoot after its initial acceleration phase during both the transients.

Considering the available dataset and the simplified equations (5), (6) and (7), a model-based identification procedure is for sure influenced by the way in which thrusts and reaction torques developed by propulsion system are estimated; in fact direct measurements of the delivered thrusts and torques are not available on Typhoon, such as on most of this kind of underwater vehicles.

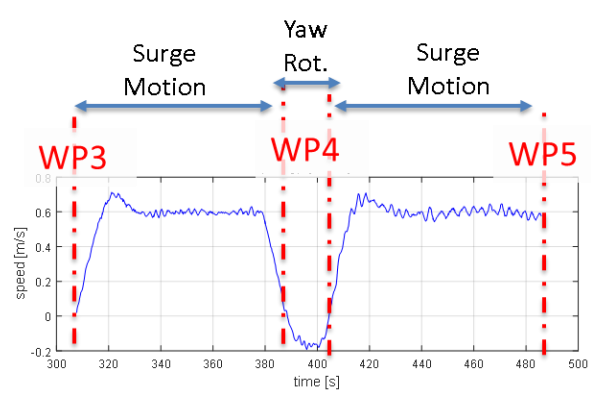

Figure 6: longitudinal vehicle speed u during the mission (measured by the board DVL)

III. Thrust Modelling and Identification

This section is organized in six paragraphs according to the following outline. Section A describes a simple model for the propeller behavior based on disc theory; the results from the theoretical model is then compared with data available in the technical literature ([14]-[16]) and discussed. In Section B a linearized model able to describe the propeller behavior in the first quadrant is given; this model overcomes some of the limits of the disc theory, but it is still too simple for the aim of the proposed work. Data from a standard propeller profile are used to derive the significant parameters of the linearized model. Taking then into account the typical torpedo-shape of many AUVs and their hovering capability, e.g. referring to Typhoon-class AUV, it is necessary to implement a more complex model able to describe a vehicle in maneuver: in Section C the model extension to four quadrant operations is thus given. At the end of this subsection, the first experimental results coming from the tests in pool of the Typhoon tunnel thrusters are given and used to tune the mathematical model.

Passing then to the interactions between the propellers and the vehicle hull and among the propellers themselves, in Section D and E other mathematical models are presented. For the effects of mutual interaction among the propellers some tuning has been done based on other experimental results at the MDM Lab, Italy.

Finally, in Section F the concept of a speed controlled actuator is proposed and discussed.

A. First Quadrant Operation: propeller behavior and simplified models

According the propeller disc theory, the pressure p corresponding to the thrust developed by an infinitesimal area of the disc is described by (8)

$$p = \frac{1}{2}\rho \;\; 2V_a\Delta_v + \Delta_v^{\;2}$$

(8)

According the simplified scheme of Figure 7, V_a represents the inlet flow speed and Δ_v the corresponding increase of axial flow velocity from the inlet to the outlet section of the propeller. In the propeller section the axial flow speed is supposed to be equal to $V_a + 0.5\Delta_v$.

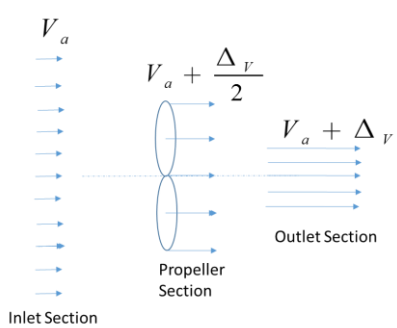

Figure 7: ideal propeller disc

From (8) it is possible to calculate the corresponding delivered thrust T under the hypothesis of uniform field of both V_a and Δ_v by integrating the corresponding pressure p developed across the disc (9):

$$T = \int_0^{d/2} p dA = \frac{1}{8}\rho\pi d^4 \;\; 2V_a\Delta_v + \Delta_v^{\;2}$$

(9)

The real propeller is treated as an ideal axial turbo-machine, in which the fluid is supposed to be ideally guided by the blades (bladed propeller disk); friction losses and blade thickness are negligible.

The corresponding speed triangle for a generic mean-line section of the propeller is represented in Figure 8:

- c_1 and c_2 are respectively the inlet and outlet absolute speed of the water;
- u is the peripheral/tangential speed of the blade, while n is the rotation speed of the propeller expressed in revolutions/second [Hz];
- w_1, w_2 are respectively the inlet and the outlet relative speed of the motor;
- α is the blade inclination with respect to the axial flow direction and is defined by (10) using the propeller pitch p and diameter d.

$$\alpha = \tan^{-1} \; p/\pi d \; = \frac{c_1}{u} = \frac{V_a}{u} \qquad (10)$$

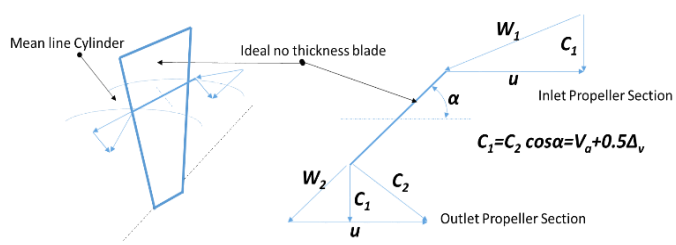

(10)

Figure 8: speed triangle of a mean-line section of the simplified bladed propeller disc

The blade is assumed to be flat (no twist applied on blade profile), dimensions of the propeller hub are negligible and finally an ideal similitude among the speed triangles of every concentric cylindrical mean-line discretizing the propeller is supposed. With these simplifications, it is possible to calculate the delivered thrust T (11) as a function of the advance coefficient J and its variation Δ_j across the propeller, which are defined respectively by (12) and (13):

$$T = \int_0^{d/2} p dA = \int_0^{d/2} \rho n^2 4r^2 \;\; 2J\Delta_j + \Delta_j^{\;2} \;\; \pi r dr =$$

$$= \pi\rho n^2 \frac{d^4}{16} \;\; 2J\Delta_j + \Delta_j^{\;2}$$

(11)

$$J = \frac{V_a}{nd}$$
(12)

$$\Delta_j = \frac{\Delta_v}{nd} \tag{13}$$

Delivered pressure p across the disc can be also calculated considering the conservation of the rothalpy across the bladed propeller disc threated as an axial turbo-machine [33] obtaining relation (14):

$$dp = \frac{1}{2}\rho \ \ w_1^2 - w_2^2 \ \ = \frac{1}{2}\rho \ \ 2V_a\Delta_v + \Delta_v^{\ 2}$$
(14)

By solving (14) the value of Δ_J as a function of the J and α can be calculated (15):

$$\Delta_J = \frac{-J\left(2+\frac{1}{\tan\alpha^2}\right)+\sqrt{J^2\left(2+\frac{1}{\tan\alpha^2}\right)^2-4\left(\frac{J^2}{\tan\alpha^2}-\pi^2\right)\left(1+\frac{1}{4\tan\alpha^2}\right)}}{2\left(1+\frac{1}{4\tan\alpha^2}\right)}$$
(15)

Once Δ_J is known the thrust T can be calculated according to (11). The corresponding results calculated in terms of propeller thrust coefficient K_t, defined according to (16), are visible in Figure 9. K_t values are functions of p/d ratio of the propeller and of the advance coefficient J. In particular, it is interesting to notice that the locus of null values of the thrust coefficient K_t corresponds to a straight line $J_{null}(p/d)$ which is analytically described by (17):

$$K_t = \frac{T}{\rho n^2 d^4}$$
(16)

$$J_{null} = p/d$$
(17)

Expression (17) can be easily justified considering that for $J=p/d$ w_1 is equal to w_2, thus expression (14) is necessary null.

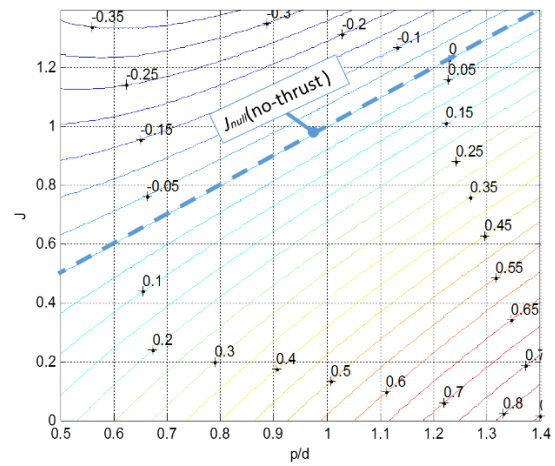

Figure 9: calculated K_t values with the bladed propeller model (perfectly guided fluid, no losses) as functions of the propeller p/d ratio and of the advance coefficient J

Considering the approximations of the bladed propeller model described above (perfectly guided fluid, no losses, negligible thickness of blades) this simplified model tends to overestimate the propeller performances, as visible in Figure 10, where the calculated bollard thrust coefficient $K_t(0)$ is compared with the corresponding values of two blade propellers of the Wageningen B-series. The behavior of the two blade propeller with a high area ratio is well approximated by the simplified model (near to perfectly guided flow). $K_t(0)$ of propellers with lower area ratio are largely over-estimated, especially for higher values of p/d ratio. **It is thus worth noting that the proposed model is suitable only for high area ratio.**

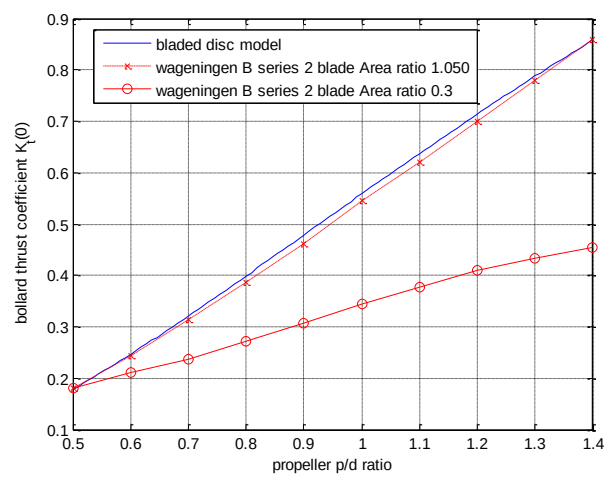

Figure 10: calculated $K_t(0)$ for bollard thrust tests (J=0) compared with the corresponding values of two blade Wageningen B-series propellers

A similar comparison could be performed as visible in Figure 11 in terms of J_{null}: the calculated value of the advance coefficient for which the delivered thrust is null is compared with the corresponding values of two propeller of the Wageningen B-series. For propellers of the same systematic

series J_{null} value is almost independent from the area ratio and is almost proportional to the propeller *p/d* ratio.

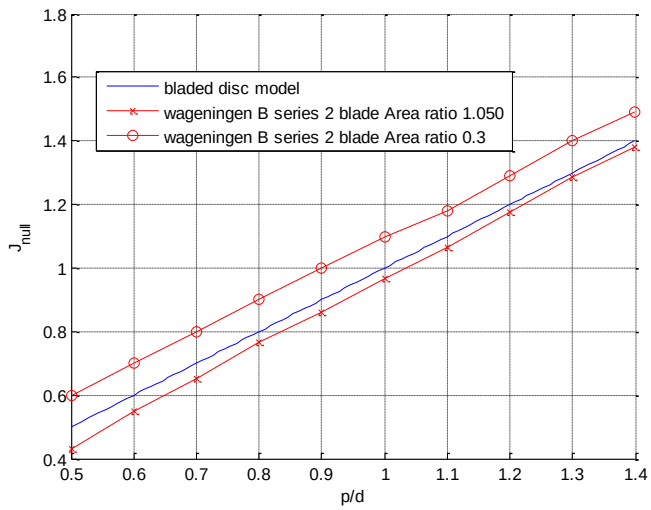

Figure 11: calculated J_{null} compared with the corresponding values of two blade Wageningen B-series propellers

B. Linearized Model

As previously seen, the bladed propeller model is partially able to reproduce the behavior of a propeller in the first quadrant:

- the thrust coefficient is a monotonically decreasing function of the propeller advance ratio;
- the bollard thrust coefficient is roughly dependent from *p/d* and area ratio for propellers of the same series;
- the value of the advance coefficient J_{null} corresponding to a null thrust coefficient is approximately proportional to the propeller *p/d* ratio.

Consequently, the behavior of the propeller K_t should be approximated by a linear function K_t^* of the advance coefficient J and of the measured bollard thrust coefficient $K_t(0)$ (18):

$$K_t^* = K_t(0)\left(1 - \frac{J}{k_{null}\ {}^{p}\!/_{d}}\right)$$

(18)

In particular, the value of the constant k_{null} should be tuned to fit the behavior of different series of propellers. As visible in Figure 12, this approach can be used to successfully approximate the behavior of ducted propeller, such as the widely diffused Kaplan Ka 4-70 propellers with 19-A nozzle [9] [14] [15]. The delivered thrust is represented as a parabolic function of n with a linear dependency from V_a (19), which is often adopted in literature [2].

$$T = \overbrace{\rho d^4 K_t(0)}^{k_{nn}} n^2 - \overbrace{\frac{\rho d^4 K_t(0)}{k_{null}\frac{p}{d}}}^{k_{nva}} V_a n = k_{nn} n^2 - k_{nva} n V_a \quad (19)$$

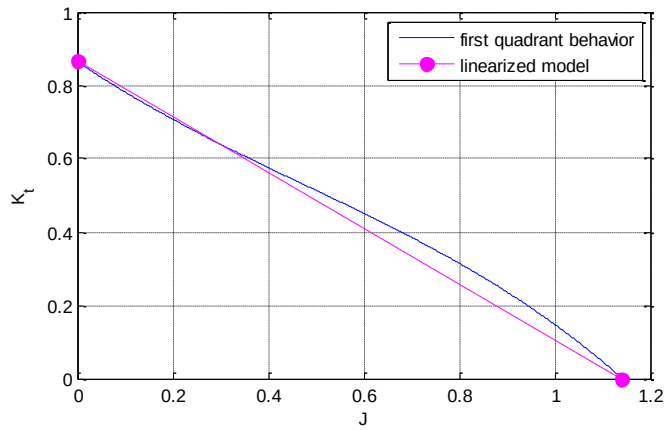

Figure 12: first quadrant operation of a ducted Ka-4-70 propeller (Nozzle 19-A) compared with the corresponding linearized model

C. Four Quadrant Operation

In order to study four quadrants operations of the propeller, the use of the advance, thrust and torque coefficients J, K_t , K_q is quite impractical. In particular null values and sign inversions of V_a and n lead to numerically inconsistent descriptions of J, K_t, K_q. For this reason, propellers advance is expressed in terms of the advance angle β defined according to (20) where the advance speed V_a is scaled with respect to the propeller tangential speed calculated at the 70% of the propeller tip radius:

$$\beta = \tan^{-1}\frac{V_a}{0.7\pi n D} = \tan^{-1}\frac{J}{0.7\pi}$$

(20)

In particular, referring to the bladed disc model β is equal to the α angle of the blade. With respect to β, thrust and torque are expressed in term of the modified coefficients C_t^* and C_q^* in which Q and T are scaled with respect to kinetic energy associated to the inlet relative speed w_{1_07} referred again to the 70% of the propeller tip radius:

$$C_t^* = \frac{T}{\left(\frac{1}{2}A_{disc}\rho w_{1_07}^2\right)} = \frac{T}{\left(\frac{\pi}{8}\rho d^2\ V_a^2 + \ 0.7 n\pi d\ ^2\right)} = \quad (21)$$

$$= \frac{T}{\left(\frac{\pi}{8}\rho d^2\ J^2 n^2 d^2 + \ 0.7 n\pi d\ ^2\right)} = \frac{T}{\rho n^2 d^4 \frac{\pi}{8}\ J^2 + 0.49\pi^2} =$$

$$= \frac{K_t}{\frac{\pi}{8}\ J^2 + 0.49\pi^2}$$

$$C_q^* = \frac{Q}{\left(\frac{1}{2}A_{disc}\rho w_{1_07}^2\right)d} = \frac{Q}{\left(\frac{\pi}{8}\rho d^2\ V_a^2 + 0.7n\pi d^{\ 2}\right)d} = \tag{22}$$

$$= \frac{Q}{\left(\frac{\pi}{8}\rho d^2\ J^2 n^2 d^2 + 0.7n\pi d^{\ 2}\right)d} = \frac{Q}{\rho n^2 d^5 \frac{\pi}{8}\ J^2 + 0.49\pi^2} =$$

$$= \frac{K_q}{\frac{\pi}{8}\ J^2 + 0.49\pi^2}$$

C_t^* and C_q^* coefficients are typically approximated in terms of Fourier series (23) whose coefficients of some widely diffused propeller series are available in literature [14] [15]. Some results for the Ka 4-70 propeller ducted in a 19-A nozzle are shown in Figure 13: the results are referred to the first 21 terms of the sum ($n=20$).

$$C_t^* = \sum_{k=1}^{n} A_k \cos\beta k + B_k \sin\beta k$$
$$C_q^* = \sum_{k=1}^{n} C_k \cos\beta k + D_k \sin\beta k \tag{23}$$

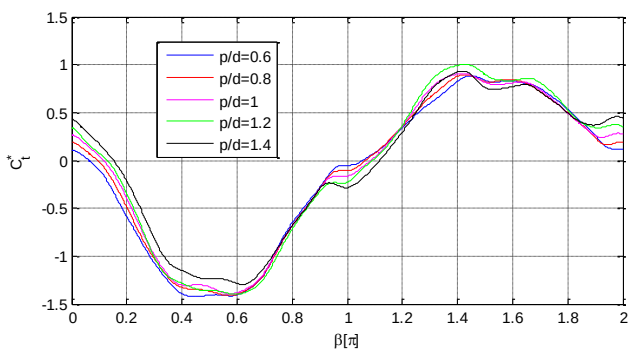

Figure 13: C_{t*} for a Ka 4-70 propeller ducted in a 19-A nozzle

In Figure 14 some experimental data concerning the bollard thrust delivered by the symmetric tunnel thrusters of Typhoon AUV are shown: the static behavior of the actuator is near to be perfectly symmetrical as it is clearly visible from the results of the tests performed in the pool of the MDM Lab in Pistoia (Italy).

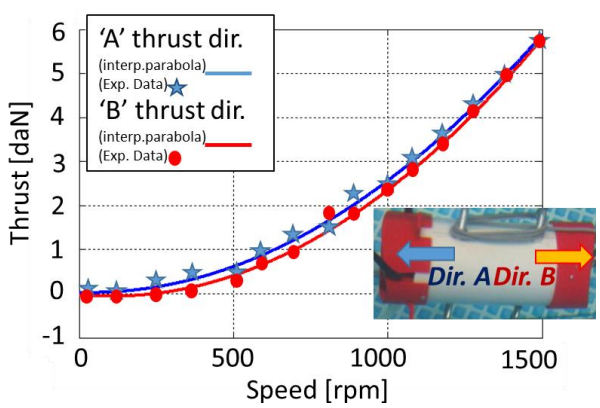

Figure 14: symmetrical behavior of Typhoon lateral thrusters. Tests performed in the MDM Lab pool [26]

The graphic of Figure 14 for a tunnel thruster should be periodic for β equal to π and consequently it can be sufficient to tabulate the behavior of the system over two quadrants. **These experimental data are thus important to start the tuning of the mathematical behavior of the Typhoon AUV propulsion system.**

D. Interaction with hull and cross flows

The interaction between the hull and the propeller behavior is a complex topic. Considering an arbitrary motion of the vehicle, the inlet flow speed of the propeller is not axial. Consequently, the values of transverse components V_{ty} V_{tz} as described in Figure 15 may be not negligible with respect to the axial one V_a.

As stated in literature, e.g. in the work of Beveridge [21], the presence of an appreciable value of cross flows V_t causes a decrease of a lateral thruster efficiency. This effect is quantified in terms of k_f, defined as the ratio between the thrust delivered with a known value of V_t and the one developed without any cross-flow disturbance.

The behavior of k_f is usually obtained interpolating experimental data with an exponential law; the value of the constant c_{loss} can be tuned to fit experimental results:

$$k_f = e^{-c_{loss}\frac{V_t^2}{T/\rho A\pi}} \tag{24}$$

Assuming a limited interaction between V_a and V_t in terms of delivered thrust it is possible to calculate the perturbed thrust T_* as proportional to the $K_t k_f$ product (25) or alternatively to C_t^* (26) for a better fit of the four quadrant behavior of the propeller:

$$T_* = k_f T = \rho n^2 d^4 K_t k_f \tag{25}$$

$$T_* = k_f T = \rho n^2 d^4 \frac{\pi}{8}\ J^2 + 0.49\pi^2\ C_t^* k_f \tag{26}$$

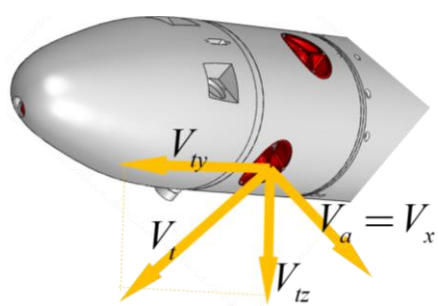

Figure 15: definition of axial and transverse flows on the thruster

Relation (26) can be mainly used for transversal tunnel thrusters of Typhoon AUV since additional effects in terms of transversal forces and torques on the thrusters produced by cross flows are neglected. In particular, it is worth noting that these terms are not negligible especially for external

propellers, often used on *ROVs*, e.g. referring to the work of Stettler et al. [24] and of Jinhyun [25].

E. Thrusters/Propellers mutual interactions

In literature there are many studies concerning the effects of mutual interactions among propellers wakes.
In particular, for actuators in series, the most relevant effects are caused by the variation of the inlet/boundary conditions of the propeller. As visible in Figure 16, the inlet speed of propeller "*B*" is perturbed by the wake of propeller "*A*". More complex 3D interactions among thrusters wakes can arise for propulsion system configurations typically adopted on ROV, as already reported in Figure 2.

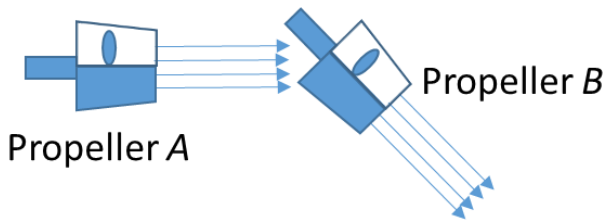

Figure 16: mutual interactions between thrusters wakes

In this work, the attention is focused on the propulsion system layout of Typhoon AUV, and, more generally, by many other torpedo-shaped AUV; for such a kind of configuration the distances between the lateral and the vertical thrusters reduce the mutual interactions.
On the other hand, Typhoon has two rear counter-rotating propellers, visible in Figure 17, and they produce appreciable transverse forces, identified using two different procedures:

- bollard thrust tests: the two main rear propellers were assembled together and tested in the MDM pool. Bollard thrusts and transversal force F_t were measured using load cells. Some results are visible in Figure 18: the transverse force is scaled with respect to the bollard thrust in the forward direction at 1500rpm. The tested propeller was a Ka 5-75 propeller in a 19-A nozzle (also for this propeller and nozzle four quadrant data are available within technical literature);

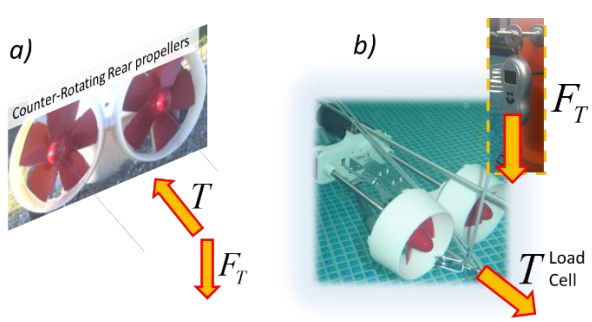

Figure 17: rear counter-rotating propellers of Typhoon AUV (a) and bollard thrust test (b) in the MDM pool (Pistoia, Italy)

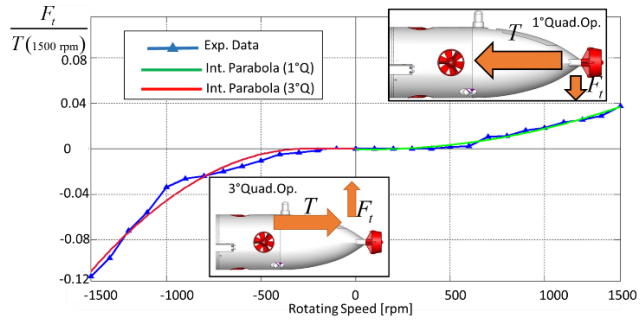

Figure 18: behavior of F_t (scaled with respect to the forward bollard thrust at 1500rpm) as a function of the propeller rotational speed

- vehicle experimental tests: Typhoon AUV has the possibility to dynamically modify the longitudinal position of its center of mass since the onboard LiPo batteries are placed on a sliding frame controlled by an electric actuator. This is visible in the scheme of Figure 19 where points G and B represent respectively the vehicle center of mass and the center of the buoyancy forces. By adjusting the longitudinal position of the batteries, the longitudinal position of the vehicle center of mass x_g changes with respect to the center of buoyancy. This way the vehicle mass distribution can be calibrated in order to satisfy static relation (27), obtained imposing the rotational equilibrium of the system drawn in Figure 19.

$$F_t x_t = G x_g \tag{27}$$

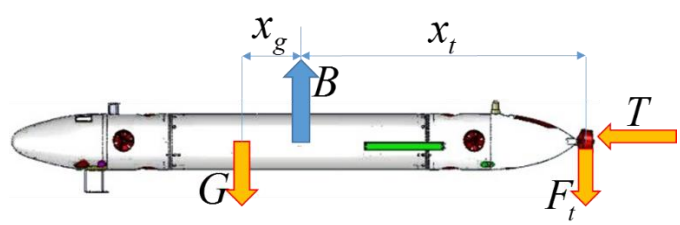

Figure 19: pitch static equilibrium

The transversal force can also be perturbed by crossflow effects so it is possible to define a perturbed value of F_t called F_{t*} defined according to (28) where k_f is the scaling factor taking into account the crossflow effects:

$$F_{t*} = k_f F_t \tag{28}$$

F. Actuation and dynamic behavior of the propulsion system

With respect to a previously fundamental work proposed by Yoerger, Cooke and Slotine [34], the authors have preferred the concept of a speed controlled actuator. This approach has been considered more useful mainly for three reasons:

- modern electric drives allow the control of a wide variety of motors, which can be quite different with respect to the brushed DC motor considered in [34];
- modern electric drives allow a direct control of the propeller speed and this solution should be preferred to a

voltage, current or torque loop, since it assures a higher robustness in terms of repeatability and stability;

- the dynamic response of the electrical system typically introduces delays that are negligible compared to the ones introduced by mechanical and hydraulic phenomena.

Most of the propellers used for small to mid-sized AUV are actuated using brushless servo-motors. As visible in the scheme of Figure 20, the motor is often coupled to a gearbox in order to fully exploit the nominal power of the motor. For DC brushless motors the torque profile Q_m can be easily approximated using the bilinear behavior of Figure 21 which corresponds to the following equations (29):

$$\begin{aligned} &if\ 0 \le \omega_m \le \omega_{nom} \Rightarrow Q_m = Q_{stall} - Q_{stall} + Q_{nom}\left(\frac{\omega_m}{\omega_{nom}}\right); \\ &if\ \omega_m > \omega_{nom} \Rightarrow Q_m = Q_{nom}\left(\frac{\omega_m - \omega_{noload}}{\omega_{nom} - \omega_{noload}}\right); \end{aligned} \tag{29}$$

In (29) Q_{nom} and Q_{stall} represent respectively the nominal and the stall torque of the motor and the torque profile is calculated as a function of the actual, the nominal and the no load speed defined as ω, ω_{nom} and ω_{noload}. For four quadrant operations a symmetric behavior is assumed for each quadrant. This assumption is generally a good approximation of the actuator behavior especially when the drive system is directly connected to the accumulator pack of the vehicle.

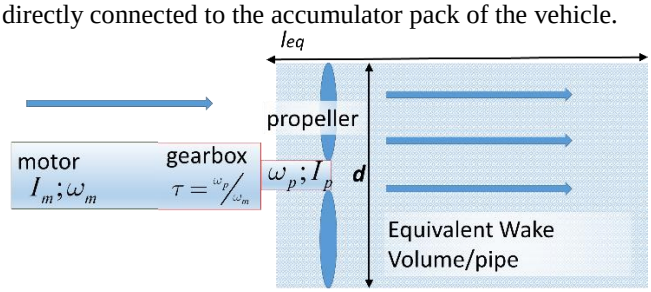

Figure 20: simplified thruster model

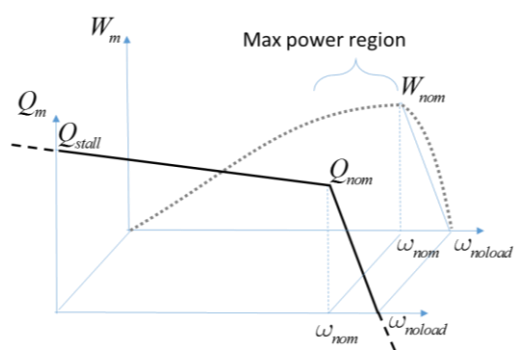

Figure 21: simplified representation of the steady state of a brushless motor in terms of delivered torque Q_m and power W_m

The dynamic behavior of the system described in Figure 20 and in Figure 21 is approximated by equation (30):

$$\left(\frac{I_m}{\tau^2} + I_p + I_{eq}\right)\dot{\omega}_p = \frac{Q_m}{\tau}\ \omega_p\ - Q\ \beta, \omega_p \tag{30}$$

In (30), the following symbols have been adopted:

- The inertia of the actuator is modelled as the sum of three contributions:
  - I_m the mechanical inertia of the motor: this term is calculated considering the reduction ratio τ due to the gearbox;
  - I_p the mechanical inertia of the propeller;
  - I_{eq} additional fluid inertia: the propeller accelerates a volume of fluid corresponding to the inertia of a cylinder of water with the same diameter d of the propeller and a height l_{eq}. I_{eq} is quite difficult to be calculated so it is approximated with the experimental test described in Figure 22. A step input in terms of reference speed is imposed to the motor and the propeller (tested in a swimming pool) and the corresponding rise time is measured. The test is repeated with different step amplitudes and the value I_{eq} which approximates the measured response of the actuator in water is estimated. It should be noticed that the value of I_{eq} calculated with this procedure could take count of additional delays caused by other phenomena, such as friction or dynamic response of the motor drive which are not considered in (30);
- The torques due to propeller load Q_p and to motor Q_m.

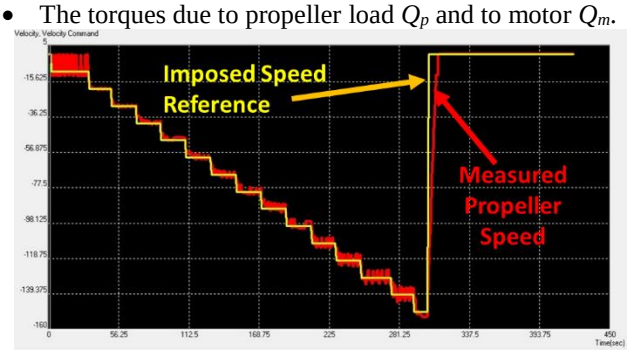

Figure 22: reference and measured propeller speed (experimental data concerning I_{eq} identification tests)

From equation (30) the maximum acceleration that can be imposed to the propeller can be calculated according to (31):

$$\dot{\omega}_{p\max} = \frac{\frac{Q_m}{\tau}\ \omega_p\ - Q\ \beta, \omega_p}{\left(\frac{I_m}{\tau^2} + I_p + I_{eq}\right)} \tag{31}$$

The reaction torque Q_r that the modelled actuator exerts to the hull can be calculated from (32), which is obtained from (30) too:

$$Q_r = \left(\frac{I_m}{\tau^2} + I_p + I_{eq}\right)\dot{\omega}_p + Q\ \beta, \omega_p \tag{32}$$

According to (31) a generic speed controlled propeller can be modelled and the simulation scheme is given in Figure 23: the reference propeller speed ω_{ref} is an input with saturated derivatives that implement the amplitude and the frequency response limitations of the actuator. Delivered thrust and reaction forces and torques can be calculated as a function of the propeller speed and of the relative advance speed with

respect to water. In particular, if four quadrant operations are considered, thrusts and reaction torques are calculated through (21) and (22) described in section III C. The effects due to the interaction with crossflows, due to the relative motions of the hull with respect to the water, are taken into account according to (24), as described in section III D. Finally, transversal forces due to the interaction with the other propellers are calculated only for the rear ones, according to the tabulated experimental results of Figure 18. *The adoption of a more simplified model for the thrust provided by the vehicle propellers only based on a quadratic function of the rotational speed induces an overestimation of the thrust itself when in motion. The decrease of the thrust with the increase of the propeller velocity w.r.t. the fluid has a consolidated evidence in the literature [9][13] also based on experimental demonstrations. The assumption of a model for the thrust simply based on the bollard behavior, overestimating the forces applied on the vehicle, translates in a consequent overestimation of the travelled distance.*

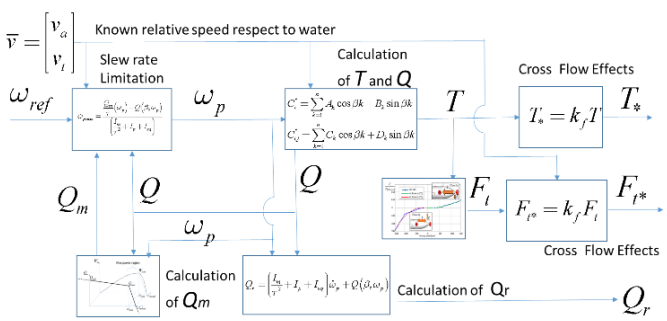

Figure 23: simulation scheme of the speed controlled propeller

IV. Calibration and Validation of the Simulation Models through Experimental Data

Most of the parameters describing the response of propellers and thrusters have been identified using experimental tests and models described in section III. Data coming from experimental campaigns, e.g. from the one described in section II, can be used to identify, calibrate and validate the parameters able to fit the hydrodynamic behavior of the vehicle hull.

The experimental data, concerning measured vehicle kinematics, coming from the sea campaign described in Figure 5 are known.

Also synchronized data concerning the rotation speed of rear propellers and thrusters are available form the field test logs.

Using the simplified model of each propeller described in Figure 23 it is possible to estimate the exerted thrust $f_i(t)$ and the reaction torque $q_i(t)$ produced by the i-th thruster/propeller. Knowing the vector $F(t)$ and $Q(t)$ of forces and torques exerted by propellers it is possible to calculate the corresponding vector estimated vector τ according to (33): it is worth noting that to take into account the transversal force caused by the interaction between the two rear propellers a seventh vector force called f_{12} is introduced.

Relations corresponding to system (33) are coherent with the scheme of Figure 24.

$$\begin{bmatrix} 1 & 1 & 0 & 0 & 0 & 0 & 0 & 0 & 0 & 0 & 0 & 0 & 0 \\ 0 & 0 & 1 & 1 & 0 & 0 & 0 & 0 & 0 & 0 & 0 & 0 & 0 \\ 0 & 0 & 0 & 0 & 1 & 1 & 1 & 0 & 0 & 0 & 0 & 0 & 0 \\ 0 & 0 & 0 & 0 & 0 & 0 & 0 & 1 & 1 & 0 & 0 & 0 & 0 \\ 0 & 0 & 0 & 0 & -\frac{l_v}{2} & \frac{l_v}{2} & l_{12} & 0 & 0 & 1 & 1 & 0 & 0 \\ -\frac{l_r}{2} & \frac{l_r}{2} & \frac{l_l}{2} & -\frac{l_l}{2} & 0 & 0 & 0 & 0 & 0 & 0 & 0 & 1 & 1 \end{bmatrix} \begin{bmatrix} F(t) \begin{Bmatrix} f_1(t) \\ f_2(t) \\ f_3(t) \\ f_4(t) \\ f_5(t) \\ f_6(t) \\ f_{12}(t) \end{Bmatrix} \\ Q(t) \begin{Bmatrix} q_1(t) \\ q_2(t) \\ q_3(t) \\ q_4(t) \\ q_5(t) \\ q_6(t) \end{Bmatrix} \end{bmatrix} = \begin{Bmatrix} \begin{bmatrix} X \\ Y \\ Z \\ K \\ L \\ M \end{bmatrix} \end{Bmatrix} \tau \qquad (33)$$

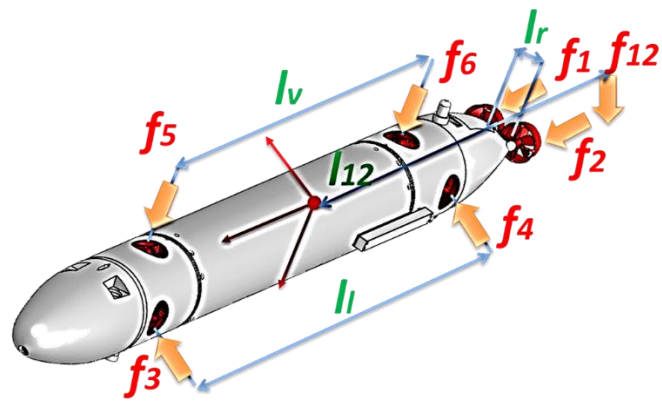

Figure 24: forces exerted by the rear propellers and the thrusters

For the proposed application, which should be treated as a constrained minimization of a functional with respect to a set of parameters (minimization based on the available experimental data - vehicle measured kinematics and propellers speeds), the authors implemented a standard least squares estimation procedure. *The result, considering that the model is linear with respect to the parameters to be identified, is obtained by exploiting the pseudo-inverse of the coefficient matrix [39]*. The optimization is performed considering admissible intervals of estimated values (hydrodynamics parameters) in order to avoid the identification of parameters with physically unfeasible or unrealistic: e.g. mass and damping parameters have to be positive real numbers and their values should not exceed a maximum value which is obtained by multiplying of a factor of ten the expected results obtained from literature [2].

This procedure was repeated for the three elementary motions (surge motion, heave motion and yaw rotation) performed during the experimental campaign obtaining the estimated values M^*_{33}, M^*_{11}, M^*_{66}, D^*_{33}, D^*_{11} and D^*_{66} given in Table I:

Table I: estimated values for the main hydrodynamic parameters

M^*_{33}	M^*_{11}	M^*_{66}	D^*_{33}	D^*_{11}	D^*_{66}
180 [kg]	180 [kg]	279 [kgm^2]	1230 [Ns^{2}m^{-2}]	58.7 [Ns^{2}m^{-2}]	1830 [Nms^2]

In particular, a simplified model independent for all the considered degrees of freedom has been adopted. In all the

cases (surge, sway and yaw motions), the considered forces acting on the vehicle are due to the vehicle propellers (control inputs) and to a quadratic drag contribution. The contributions to the dynamics due to the added inertia, as well as all the other hydrodynamic phenomena, are not considered in the proposed model in coherence with the aim of the work that is targeted to the definition of a procedure for the identification of a simplified model based on the main Hydrodynamic Parameters from a reduced experimental dataset. **M^*_{33} and M^*_{11} are the static mass of the vehicle; the identified values are coherent with the AUV's mass, of about 180kg. In the performed calculation of M^*_{33} and M^*_{11} it has been assumed to identify the same value, since from a physical viewpoint they represent the same quantity, the static mass of the mobile robot.**

In order to validate the performed identification, the authors inserted the identified parameters in a 3D model of the vehicle, developed in Matlab-Simulink™ with following features:

- Hull dynamics described implementing (1). The number of known parameters needed to fully implement (1) is for sure higher than the six identified values given in Table I. However, for the missing parameters the authors adopted common assumptions: **M_{11}, M_{22} and M_{33} are supposed to be equal (as abovementioned)**, while extra-diagonal terms of the matrix are supposed to be null (axial symmetry of inertial properties with respect to longitudinal direction). For the other unidentified parameters, e.g. D_{44}, the literature source [2] is adopted to calculate near to realistic values;
- The estimated forces $\tau(t)$ are calculated according to the model described in Figure 20 and using as input the measured/recorded rotational speeds of the propellers.

The simulated trajectory of the full three-dimensional model imposing the same input speeds of the propellers is then compared with the known, experimental one.

As visible in Figure 25 there is a very good matching between the experimental and the simulated vehicle trajectory; this is true also considering unmodelled or partially unknown disturbances, such as (weak) marine currents that were present during the experimental test. **The absolute error between the simulated and the experimental trajectory is reported in Table II: for the travelled distance under study, equal to about 70 m, the mean error is 1.2 m.** There is also a good agreement in terms of qualitative shape of the trajectory: as visible in the detail of Figure 26, it is quite clear the capability of the model to fit the transient behavior in correspondence of WP4 vertex where the vehicle performs a sudden deceleration followed by a yaw rotation of 90° and then by an acceleration. **Since the comparison between the trajectories, the real one at sea and the simulated one, is made with the same control inputs, i.e. the propellers rotations, the achieved matching highlights the good identification of the vehicle parameters.**

Finally, it is worth noting that the identified values of some parameters, such as the longitudinal viscous coefficient D_{11} and the vertical one D_{33}, correspond to feasible values of hydraulic drag coefficients according to [35] [36].

In particular, considering the transversal section of the vehicle the equivalent longitudinal drag coefficient C_{DX} calculated from the identified value D_{11} is equal to 0.09: a value coherent with correlations suggested by [35]. For the calculation of the longitudinal drag coefficient both contributions of form and friction resistances were considered: for Typhoon AUV, taking into account its length/volume ratio, the second term (the friction one) is dominant. The calculation of these losses is very sensitive to the value of the Reynolds number and thus when the speed of the vehicle is relatively low, e.g. around one knot, the coefficient is a bit underestimated (it is likely around 0.1). On the other hand, the vehicle is able to reach a maximum speed of about 6 knots: in this case, a reduction of the friction coefficient to about 0.08 is expected. The current identified value can be considered in accordance with the literature [35] and relatively accurate for a speed range between 1 and 4 knots.

Also for the heave coefficient, the equivalent vertical drag coefficient C_{DZ} assumes the value of 1.09, identified from D_{33}, and it is in accordance with the corresponding value given by [36] as visible in Figure 27: Typhoon AUV has a slightly higher losses with respect to the ideal value present in literature. However, it should be considered the presence of additional drag surfaces on the vehicle (such as the antenna and some sensors out of its main shape).

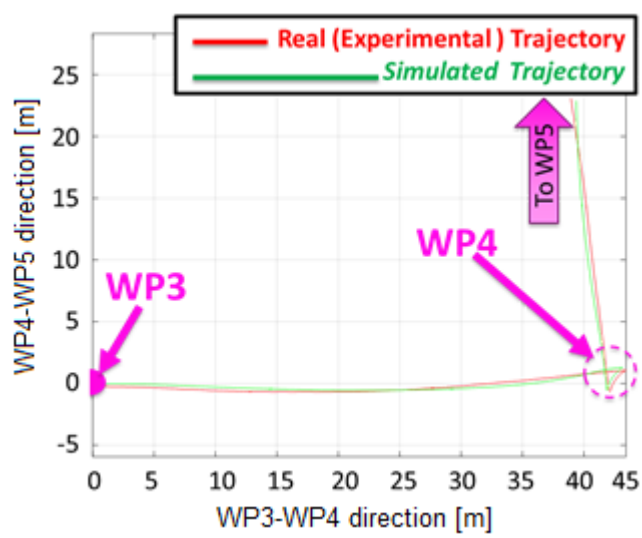

Figure 25: comparison between the simulated and the experimental trajectory of Typhoon AUV

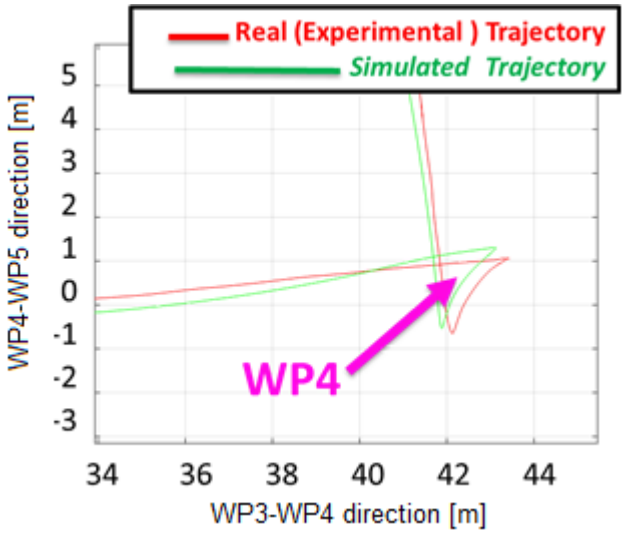

Figure 26: detail of the comparison between the simulated and the experimental trajectory of Typhoon AUV, in correspondence of WP4

Table II: Statistical Distribution of the absolute error between the simulated and the measured trajectory

Mean Error [m]	Max Error[m]	Standard Dev.[m]
1.2	2.4	1.7

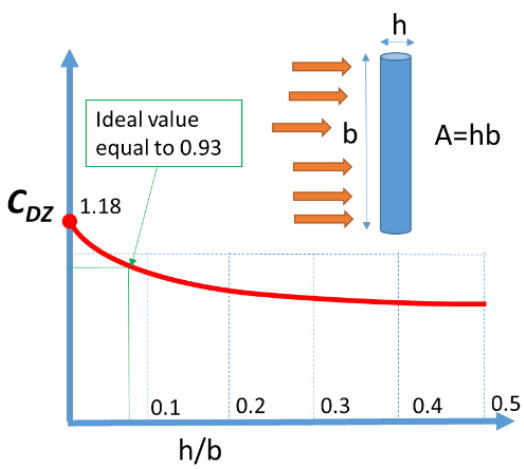

Figure 27: ideal behavior of C_{DZ}, according to [36]

V. Conclusions and Future Developments

In this research work, a rapid procedure for a fast calibration of the main hydrodynamic parameters of an AUV is proposed. The procedure has been successfully validated using simulation tools and the experimental data coming from campaigns at sea.

Future developments are scheduled, e.g. a considerable part of the identification work performed on thrusters could be simplified adopting smart drive system for the propellers: preliminary studies about this have been proposed and implemented by the authors in the next generation of AUVs the University of Florence have built [32]. Research work is still ongoing but these smart, customized drive systems are able to estimate online many useful parameters such a torque, delivered thrust, estimated advance coefficient.

Another aspect that will be further improved is the tuning of other hydrodynamic coefficients describing the general vehicle dynamics, in compliance with (1) [2].

VI. References

[1] Dsds Paull, L., Saeedi, S., Seto, M., & Li, H. AUV navigation and localization: A review. Oceanic Engineering, IEEE Journal of, 39(1), 131-149, 2014.

[2] Fossen, T. I. Guidance and Control of Ocean vehicles, Wiley, ISBN 0-471-94113-1, 1994.

[3] Bruce R. Munson, Theodore H. Okiishi, Wade W. Huebsch, Alric P. Rothmayer, *Fundamentals of Fluid Mechanics – 7th edition*, John Wiley & Sons, USA, 2013.

[4] S. F. Hoerner, Fluid-Dynamic Drag, Practial information on aerodynamic drag and hydrodynamic resistence, Hoerner, United Kindgom, 1965.

[5] Suzuki, H., Yoshida, H., Inoue, T., Watanabe, Y., & Sakaguchi, J. Evaluation of Methods to Estimate Hydrodynamic Force Coefficients of Underwater Vehicle Based on CFD. In Control Applications in Marine Systems, Vol. 9, No. 1, pp. 197-202, 2013.

[6] Zare Ernani, M., Bozorg, M., & Ebrahimi, S. Identification of an Autonomous Underwater Vehicle Dynamic Using Extended Kalman Filter with ARMA Noise Model. International Journal of Robotics, 4(1), 22-28, 2015.

[7] Van De Ven, P. W., Johansen, T. A., Sørensen, A. J., Flanagan, C., & Toal, D. Neural network augmented identification of underwater vehicle models. Control Engineering Practice, 15(6), 715-725, 2007.

[8] Miskovic, N., Vukic, Z., Barisic, M., & Soucacos, P. P. AUV identification by use of self-oscillations. In Control Applications in Marine Systems, Vol. 7, No. 1, pp. 181-186, 2007.

[9] Carlton J. Marine propellers and propulsion. 2nd ed. Elsevier, 2007.

[10] Rhee, Shin Hyung, and Shitalkumar Joshi. "Computational validation for flow around a marine propeller using unstructured mesh based Navier-Stokes solver." JSME International Journal Series B 48.3, 562-570, 2005.

[11] Chen, Bin, and Frederick Stern. "Computational fluid dynamics of four-quadrant marine-propulsor flow." Journal of Ship Research 43.4, 218-228, 1999.

[12] Riccardo Broglia, Giulio Dubbioso, Danilo Durante, Andrea Di Mascio, Simulation of turning circle by CFD: Analysis of different propeller models and their effect on manoeuvring prediction, Applied Ocean Research 39, 1–10, 2012.

[13] Pivano, Luca, and Tor Arne Johansen. "A four-quadrant thrust estimation scheme for marine propellers: Theory and experiments." Control Systems Technology, IEEE Transactions on 17.1, 215-226, 2009.

[14] Oosterveld MWC. Wake adapted ducted propellers. Wageningen: Netherlands Ship Model Basin (NSMBPublication No. 345), 1970.

[15] Oosterveld MWC. Ducted propeller characteristics. In: RINA symposium on ducted propellers, London, 1973.

[16] The Wageningen C- and D-Series Propellers J.Dang/H.J.J.vdBoom/J.Th.Ligtelijn, FAST, 2013, the 12th International Conference on Fast Sea Transportation, Amsterdam, 2-5 Dec. 2013.

[17] Yoerger DR, Cooke JG and Slotine JE. The influence of thruster dynamics on underwater vehicle behavior and their incorporation into control system design. IEEE J Oceanic Eng 15(3): 167–178, 1990.

[18] Ferri, G., Manzi, A., Fornai, F., Ciuchi, F., & Laschi, C. (2013, June). A systematic method for dynamic modeling and identification of a small-sized autonomous surface vehicle using simulated annealing techniques. In OCEANS-Bergen, 2013 MTS/IEEE (pp. 1-9). IEEE, 2013.

[19] Chislett, M.S. and O. Björheden, Influence of ship speed on the effectiveness of a lateral-thrust unit. Report Hy-8, Hydro-og Aerodynamisk Laboratorium, Lyngby, Denmark, 1966.

[20] Alistair Palmer, Grant E. Hearn, Peter Stevenson, Modelling Tunnel Thrusters for Autonomous Underwater Vehicles, Proc., IFAC workshop on navigation, guidance and control of underwater vehicles, Killaloe, Ireland, 2008.

[21] Beveridge, J.L. 'Design and Performance of Bow Thrusters'. Marine Technology, 9(4), 439-453, 1972.

[22] Furlong, M. System identification of the hydrodynamic characteristics of underwater vehicles. Engineering Doctorate Thesis, University of Southampton, 2005.

[23] Saunders, A. & M. Nahon The effect of forward vehicle velocity on through-body AUV tunnel thruster performance. In: MTS/IEEE Oceans 2002 – marine frontiers, Biloxi, MI, USA, 29-31 Oct. 2002. IEEE,Piscataway, NJ, USA, 2002.

[24] Stettler, J. W., Hover, F. S., & Triantafyllou, M. S. Preliminary results of testing on the dynamics of an azimuthing podded propulsor relating to vehicle maneuvering. In Proc. of the 1st International Conference on Technological Advances in Podded Propulsion, University of Newcastle, UK (pp. 321-33), 2004.

[25] Jinhyun Kim, Wan Kyun Chung, Accurate and practical thruster modeling for underwater vehicles, Ocean Engineering 33, 566–586, 2006.

[26] Allotta, B., Pugi, L., Bartolini, F., Ridolfi, A., Costanzi, R., Monni, N., Gelli, J. Preliminary design and fast prototyping of an Autonomous Underwater Vehicle propulsion system, Proceedings of the Institution of Mechanical Engineers Part M: Journal of Engineering for the Maritime Environment, 229 (3), pp. 248-272, 2015.

[27] Curtis TL, Perrault D, Williams C, et al. C-SCOUT: a general-purpose AUV for systems research. In: Proceedings of the 2000 international symposium on underwater technology 2000 (UT '00), Tokyo, Japan, 23–26 May 2000, pp.73–77. New York: IEEE.

[28] Stokey RP, Roup A, von Alt C, et al. Development of the REMUS 600 autonomous underwater vehicle. In: Proceedings of MTS/IEEE OCEANS, 2005, Washington, DC, 17–23 September 2005, vol. 2, pp.1301–1304. New York: IEEE.

[29] Whitney, J. W., and S. M. Smith. "Observations on the dynamic performance of tunnel thrusters." OCEANS'98 Conference Proceedings. Vol. 2. IEEE, 1998.

[30] A B Phillips, L. Steenson, C. Harris, E.Rogers, S. R. Turnock, M. Furlong, Delphin2: An over actuated autonomous underwater vehicle for manoeuvring research,Trans RINA, Vol 151, Part A1, Intl J Maritime Eng, 2009.

[31] Allotta,B., Baines, S., Bartolini, F., Bellavia, F., Colombo, C., Conti, R., Costanzi, R.,Dede, C., Fanfani, M., Gelli, J., Gundogdu, H.T., Monni, N., Moroni, D., Natalini, M., Pascali, M.A., Pazzaglia, F., Pugi, L., Ridolfi, A., Reggiannini, M., Roig, D., Salvetti, O., Tekdemir, E.I. Design of a modular Autonomous Underwater Vehicle for archaeological investigations, MTS/IEEE OCEANS 2015 - Genova: Discovering Sustainable Ocean Energy for a New World, Genova, Italy, 2015.

[32] Allotta, B., Costanzi, R., Gelli, J., Paolucci, L., Pugi, L., Ridolfi, A. Development and testing of the propulsion system of Marta AUV, MARINE 2015 - Computational Methods in Marine Engineering VI, pp. 646-657, 2015.

[33] G. Manfrida, S. Stecco Le Turbomacchine, Pitagora Editrice, 1993.

[34] Yoerger DR, Cooke JG and Slotine JE. The influence of thruster dynamics on underwater vehicle behavior and their incorporation into control system design. IEEE J Oceanic Eng 15(3): 167–178, 1990.

[35] Munson B.R., Okiishi T.H., Huebsch W., Rothmayer A., *Fundamentals of Fluid Mechanics*, Wiley.

[36] Hoerner S.F., Fluid-Dynamic Drag: Practical information on aerodynamic drag and hydrodynamic resistance, 1965.

[37] Allotta B., Costanzi R., Ridolfi A., et al., The ARROWS project: adapting and developing robotics technologies for underwater archaeology. In: Proceedings of the IFAC Workshop on Navigation, Guidance and Control of Underwater Vehicles (NGCUV2015). IFAC - International Federation of Automatic Control, Girona, Spain, 28-30 April 2015.

[38] Allotta B., Costanzi R., Fanelli F., Monni N., Ridolfi A., Single axis FOG aided attitude estimation algorithm for mobile robots. MECHATRONICS, vol. 30, p. 158-173, 2015.

[39] Siciliano B., Sciavicco L., Villani L., Oriolo G. Robotics – Modelling, planning and control, Springer, ISBN 978-1-84628-641-4, 2009.